Scientific Research Publishing

Open Journal of Applied Sciences, 2026, 16(1), 143-167
https://www.scirp.org/journal/ojapps
ISSN Online: 2165-3925
ISSN Print: 2165-3917

A Real-Time Locational Marginal Pricing Strategy for Smart Grids Based on Demand-Side Management

Haolong Wu, Yan Gao*

School of Management, University of Shanghai for Science and Technology, Shanghai, China
Email: 18110236810@163.com, *gaoyan@usst.edu.cn

How to cite this paper: Wu, H.L. and Gao, Y. (2026) A Real-Time Locational Marginal Pricing Strategy for Smart Grids Based on Demand-Side Management. *Open Journal of Applied Sciences*, **16**, 143-167.
https://doi.org/10.4236/ojapps.2026.161010

Received: December 13, 2025
Accepted: January 9, 2026
Published: January 12, 2026

Abstract

With the widespread integration of high-penetration renewable energy, load volatility and spatio-temporal imbalances in power systems have intensified, imposing higher demands on real-time supply-demand balance. Traditional real-time pricing mechanisms often neglect the physical constraints of distribution networks, resulting in dispatch schemes that may be infeasible in practical grid operations. Meanwhile, locational marginal pricing mechanisms typically assume inelastic loads, failing to effectively integrate demand-side response from users. To simultaneously enhance the economic efficiency and physical feasibility of grid operation, this paper designs a real-time locational marginal pricing strategy integrated with demand-side management. A Bi-level optimization framework based on the Stackelberg game is constructed: the upper level aims to maximize the profit of electricity suppliers, employing a power flow model based on the DistFlow equations and utilizing second-order cone relaxation techniques to accurately characterize physical constraints such as grid congestion, losses, and voltage limits. The lower level seeks to maximize consumer welfare, establishing a convex optimization response model that incorporates distributed energy resources, energy storage, and user electricity utility. By applying the Karush-Kuhn-Tucker (KKT) conditions and duality theory, the lower-level problem is transformed into constraints for the upper level, ultimately forming a mixed-integer linear programming model that can be efficiently solved. Simulation results validate the rationality and effectiveness of the proposed pricing mechanism in promoting renewable energy accommodation and enhancing overall system welfare.

Keywords

Smart Grid, Demand Side Management, Real-Time Pricing, Locational

Marginal Pricing, Bi-Level Optimization, Supply-Demand Balance

1. Introduction

Global electricity demand continues to grow, particularly driven by accelerated industrialization, urbanization, and the large-scale integration of renewable energy. This trend imposes higher requirements for real-time balance in power systems. Due to the unique operational characteristic that "supply and demand must be balanced in real time", any deviation may trigger frequency fluctuations, voltage instability, or even severe consequences such as large-scale blackouts [1]. Furthermore, supply-demand imbalances increase system scheduling costs and reduce resource utilization efficiency, weakening the overall economic benefits of the electricity market. Therefore, achieving dynamic coordination of supply and demand through effective market mechanisms has become a core issue urgently needing solution in the power industry.

Demand Response (DR), as a vital tool for demand-side management, aims to achieve supply-demand balance [2]. Its core mechanism is price response [3], which encourages users to effectively manage their power consumption by establishing effective pricing mechanisms. Currently, common pricing models include fixed pricing [4], Time-of-Use (TOU) pricing [5], Critical Peak Pricing (CPP) [6], and Real-Time Pricing (RTP) [7]. Among these, real-time pricing is widely considered the most promising mechanism [8]. RTP not only mitigates the spatio-temporal load imbalances exacerbated by the large-scale integration of distributed photovoltaics (PV), energy storage systems (ESS), and electric vehicles but also guides users to adjust their consumption behaviors through dynamic price signals, thereby relieving grid operational pressure and enhancing resource utilization efficiency [9]-[14].

Reference [15] first proposed the concept of RTP. Since then, related research has mainly focused on two perspectives: the openness of the electricity market and the attribute of electricity as a public good, typically analyzed through equilibrium methods. Current research on real-time pricing mechanisms falls into two main categories: one seeks optimal dispatch using social welfare maximization methods; the other investigates the equilibrium between supply and demand using bi-level optimization and game theory. The social welfare maximization method, based on shadow price theory, aims to promote fair resource allocation to achieve high-level social equity and theoretically optimize total social welfare [16]. Reference [17] first applied social welfare maximization as a pricing objective to smart grid real-time pricing, using duality methods to solve the optimization model. Additionally, the Karush-Kuhn-Tucker (KKT) method [18] [19] and the Alternating Direction Method of Multipliers (ADMM) [20] [21] are effective methods for solving social welfare maximization models. Bi-level optimization and game theory models can effectively describe systems with hierarchical structures, satisfying the interests of both supply and demand sides, and obtaining real-time prices by

directly solving the model [22] [23]. For instance, Reference [24] proposed a two-stage hybrid DR strategy based on bi-level optimization to solve power consumption deviation problems in multi-energy generation systems, minimizing the difference between actual and ordered energy consumption. Reference [25] formulated an RTP strategy to address uncertainty in two-level microgrids, obtaining optimal prices using KKT conditions, smoothing methods, and a rolling penalty function algorithm. From the perspective of pricing dimensions, the aforementioned RTP mechanisms mainly address dynamic equilibrium in the time scale, guiding users to shift loads across different periods via time-varying price signals. However, traditional RTP typically employs a unified system clearing price, ignoring differences in power supply costs caused by spatial factors such as network congestion and line losses. Consequently, the feasibility of these dispatch results in practical systems is insufficient.

Locational Marginal Pricing (LMP) is the most efficient spatial pricing method in power systems [26]. As a mature pricing mechanism, it calculates independent prices for each node while considering grid physical characteristics, thereby reflecting the true cost of electricity at different geographical locations. The theoretical basis of LMP stems from the Optimal Power Flow (OPF) model, which determines nodal prices by solving non-linear optimization problems. Existing studies indicate that LMP can not only improve market operational efficiency but also promote optimal resource allocation [26] [27]. Compared to single-price mechanisms, LMP more accurately characterizes economic and technical constraints in power transmission and is thus widely applied in North American and European power markets [28] [29]. However, traditional LMP often assumes rigid loads, failing to effectively incorporate the collaborative optimization of user price response and distributed resources [30] [31]. Meanwhile, LMP struggles to reflect the dynamics of the supply-demand game when facing uncertainties brought by high-penetration renewable energy integration [32] [33].

To address the above problems, this paper proposes a bilevel real-time pricing strategy combining demand-side management with LMP. The upper level is based on the DistFlow power flow model and handles grid physical constraints through Second-Order Cone Programming (SOCP) relaxation; the lower level constructs a user response model including distributed PV, energy storage, and flexible loads. This bilevel optimization framework more realistically reflects electricity market characteristics: the supply side acts as the leader, publishing real-time nodal prices, while the demand side acts as the follower, adjusting load curves according to prices, forming a closed loop of "price signal transmission - load response feedback". By introducing KKT conditions and strong duality theory, the model is further transformed into a Mixed-Integer Linear Programming (MILP) problem, enabling efficient solution.

2. System Framework

Consider a power transmission network connected to the main grid, containing

multiple generation units and multiple microgrids. The generation units at each node are uniformly dispatched by the Power Market Scheduling Center (PMSC), In this framework, the PMSC acts as the independent system operator and market coordinator, holding the primary authority to maintain grid stability and economic efficiency. As the leader in the proposed Stackelberg game, the PMSC possesses global knowledge of the network topology and physical constraints, allowing it to determine the optimal power supply plan and publish real-time locational marginal prices (LMP) to guide subordinate demand-side responses. Each microgrid connects a certain number of users, and each user is equipped with small-scale distributed renewable energy generation equipment and an Energy Storage System (ESS). Additionally, users have embedded bidirectional smart meters to receive price signals from their respective nodes and optimize their electricity consumption strategies accordingly.

The system structure is shown in Figure 1. Within each scheduling cycle, the PMSC first publishes price signals to microgrid users. Users then adjust their

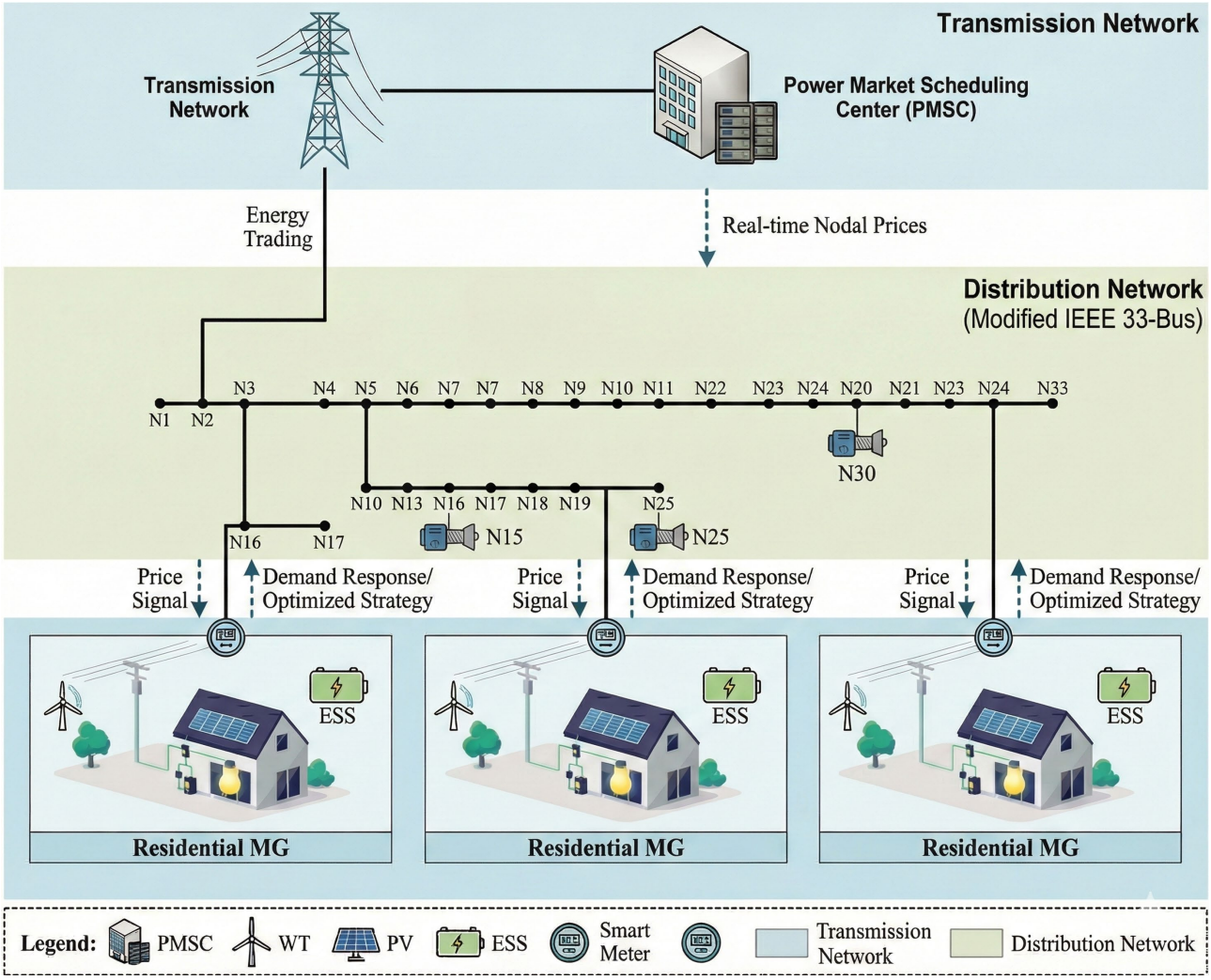

Figure 1. Schematic diagram of the simulation system.

consumption behavior based on this price information, thereby realizing a price-based demand response mechanism.

Let the set of nodes be denoted by cc. The set of microgrid users connected to a specific node i is denoted by $\mathcal{N}_i^{MG} = \{1, \cdots, N_i^{user}\}$, where $n \in \mathcal{N}_i^{MG}$ represents the n-th user at node i. Similarly, the set of generators at node i is denoted by $\mathcal{N}_i^G$. The set of transmission lines in the power system is denoted by $\mathcal{L} = \{1, \cdots, N^L\}$. Assume one day acts as an operation cycle, divided into T time slots, denoted as $t \in \mathcal{T} = \{1, 2, \cdots, T\}$.

3. System Model

3.1. Demand Side

In the electricity market, the objective of users is to maximize their individual welfare by adjusting power consumption and managing renewable energy generation and energy storage systems. It is assumed that the electricity supplier can fully meet the power demand of all users.

3.1.1. Utility Function

The utility function is a concept from microeconomics that establishes a mathematical relationship between the quantity of commodity consumption and consumer subjective satisfaction. In power systems, user energy consumption behavior can be characterized by a quadratic utility function. This function adheres to the law of diminishing marginal utility and exhibits concavity, where marginal utility slows down as consumption increases, eventually stabilizing at a saturation point. While various forms such as logistic and logarithmic functions exist, this paper adopts the quadratic utility function, as it effectively captures the principle of diminishing marginal utility. This choice is widely recognized in power system economics for accurately representing rational consumer satisfaction while maintaining computational tractability for optimization [17]. This paper adopts the quadratic utility function. For a user n located at node i ($n \in \mathcal{N}_i^{MG}$, $i \in \mathcal{N}$) during time slot t, the utility function $U_{i_n,t}^{MG}$ is defined as a piecewise function:

$$U_{i_n,t}^{MG} = \begin{cases} \omega_{i_n,t} P_{i_n,t}^L - \dfrac{\alpha}{2}\left(P_{i_n,t}^L\right)^2, 0 \le P_{i_n,t}^L \le \dfrac{\omega_{i_n,t}}{\alpha} \\ \dfrac{\left(\omega_{i_n,t}\right)^2}{2\alpha}, P_{i_n,t}^L > \dfrac{\omega_{i_n}^t}{\alpha} \end{cases} \tag{1}$$

where $P_{i_n,t}^L$ is the active power consumption of user n at node i in time slot t. $\omega_{i_n,t}$ and α are non-negative preset parameters. $\omega_{i_n,t}$ represents the basic demand intensity, and α characterizes the rate of diminishing marginal utility. Assuming users operate within the non-saturated region, the load is subject to lower and upper limit constraints:

$$P_{i_n}^{L,\min} \le P_{i_n,t}^L \le P_{i_n}^{L,\max} \tag{2}$$

where $P_{i_n}^{L,\min}$ and $P_{i_n}^{L,\max}$ are the minimum and maximum power consumption limits for user n at node i.

3.1.2. Distributed Renewable Energy

In power systems, the distributed renewable energy equipment equipped by users is typically small-scale, such as rooftop photovoltaics (PV) or small wind power generation devices, primarily used to meet the user's own electricity demand. Given their limited installed capacity, the generated energy is usually not sold back to the grid and is limited to self-consumption.

For small-scale renewable energy output, a deterministic generation curve is adopted, fitted through historical data or generated from typical scenarios, to maintain model accuracy while ensuring computational efficiency. Assuming the PV generation quantity $P_{i_n,t}^{RES}$ is an exogenous parameter satisfying the constraint: $P_{i_n,t}^{RES} \in \left[0, P_{i_n,t}^{RES,\max}\right]$, where $P_{i_n,t}^{RES,\max}$ is the maximum PV generation capability in time slot t. Assuming the generation cost of renewable energy is negligible, the maintenance and depreciation loss costs of the renewable energy generation system should still be accounted for, modeled using a quadratic function [34]:

$$\begin{aligned} C_{i_n,t}^{RES} &= \gamma_{i_n}^{RES} P_{i_n,t}^{RES} + \delta_{i_n}^{RES} \left(P_{i_n,t}^{RES}\right)^2 \\ 0 \le P_{i_n,t}^{RES} &\le P_{i_n,t}^{RES,\max} \end{aligned} \tag{3}$$

where $\gamma_{i_n}^{RES}$ and $\delta_{i_n}^{RES}$ are non-negative preset parameters.

3.1.3. Energy Storage System

Energy Storage Systems (ESS) play a key role in power management by smoothing electricity costs through flexible charging and discharging strategies and enhancing the stability and reliability of power supply. Their dynamic behavior and related characteristics are modeled as follows:

1) Charging and Discharging Dynamics

The capacity state of the ESS changes over time. Its update equation and related constraints are:

$$\begin{aligned} &E_{i_n,t} = E_{i_n,t-1} + \Delta t P_{i_n,t}^{ESS} \\ &E_{i_n}^{\min} \le E_{i_n,t} \le E_{i_n}^{\max} \\ &-P_{i_n}^{ESS,\max} \le P_{i_n,t}^{ESS} \le P_{i_n}^{ESS,\max} \\ &\sum_{t=1}^{T} \Delta t P_{i_n,t}^{ESS} = 0 \end{aligned} \tag{4}$$

where $P_{i_n,t}^{ESS}$ is the charging or discharging power of the storage device in time slot t. When $P_{i_n,t}^{ESS} > 0$, it indicates charging; when $P_{i_n,t}^{ESS} < 0$, it indicates discharging. $E_{i_n,t}$ represents the energy storage capacity state in time slot t, reflecting the remaining power of the storage device. $E_{i_n}^{min}$ and $E_{i_n}^{max}$ are the minimum and maximum capacities of the ESS. $P_{i_n}^{ESS,\max}$ is the maximum power limit for charging (or discharging), which is a preset parameter ensuring that charging and discharging operations are performed within the power range the device can withstand. The equation $\sum_{t=1}^{T} \Delta t P_{i_n,t}^{ESS} = 0$ represents the periodic constraint for

storage scheduling.

2) Charging and Discharging Costs

The operating cost of the ESS mainly stems from equipment depreciation and maintenance, which is related to the amount of charging and discharging energy. It is modeled using the following function [22]:

$$C_{i_n,t}^{ESS} = \gamma_{i_n}^{ESS} P_{i_n,t}^{ESS} + \delta_{i_n}^{ESS} \left(P_{i_n,t}^{ESS} \right)^2 \tag{5}$$

where $\gamma_{i_n}^{ESS}$ and $\delta_{i_n}^{ESS}$ are non-negative preset parameters.

3.1.4. Total Welfare of Demand Side

Considering users equipped with distributed photovoltaics and energy storage, their total welfare consists of electricity utility minus electricity purchase costs, renewable energy equipment maintenance costs, and energy storage operating costs. The net power purchased by the user from the grid is:

$$P_{i_n,t}^{MG} = P_{i_n,t}^{ESS} + P_{i_n,t}^{L} - P_{i_n,t}^{RES} \tag{6}$$

where $P_{i_n,t}^{MG}$ is the power purchased by the user from the grid in time slot t, representing the interaction power. $\lambda_{i,t}$ is the real-time electricity price at node i in time slot t. To prevent market disorder caused by excessively low or high electricity prices, upper and lower limit constraints are applied to the electricity price:

$$\lambda_{i,t}^{\min} \le \lambda_{i,t} \le \lambda_{i,t}^{\max} \tag{7}$$

where $\lambda_{i,t}^{min}$ and $\lambda_{i,t}^{max}$ are preset parameters.

The objective function of the demand side is to maximize total welfare, which can be formulated as:

$$\begin{gathered} \max \sum_{t=1}^{T} \left(U_{i_n,t}^{MG} - C_{i_n,t}^{RES} - C_{i_n,t}^{ESS} - C_{i_n,t}^{EX} \right) \\ C_{i_n,t}^{EX} = \lambda_{i,t} P_{i_n,t}^{MG} \end{gathered} \tag{8}$$

For ease of subsequent solution, this is transformed into:

$$\min \sum_{t=1}^{T} \left(-U_{i_n,t}^{MG} + C_{i_n,t}^{RES} + C_{i_n,t}^{ESS} + C_{i_n,t}^{EX} \right) \tag{9}$$

where the first term is negative utility, the second and third terms are photovoltaic maintenance costs and energy storage operating costs respectively, and the fourth term is the electricity purchase cost.

3.2. Supply Side

In the power market scheduling system, after collecting and integrating all users' consumption data, the system's objective is to maximize the overall profit of the generation side by optimizing electricity prices and power supply dispatch schemes. To achieve this, the system needs to ensure that the total generation complies with distribution network power flow constraints while satisfying total user demand, guaranteeing the feasibility of power transmission and the safe and stable opera-

tion of the grid. Furthermore, it is necessary to coordinate pricing strategies and generation plans to maximize profits based on supply-demand balance and improve system operational efficiency.

3.2.1. Power Transmission Loss Cost

The DistFlow power flow model is widely used in radial distribution network analysis [35]. Based on branch power, this model is more suitable for radial distribution systems compared to traditional node-power-based methods. In this model, power losses must be accurately calculated based on node voltage magnitudes, line resistance, and reactance. For the line l_{ij} connecting node i and node j, denote ij as the corresponding line l_{ij}. The basic power flow equations are as follows [36]:

$$\begin{aligned} U_{j,t}^2 &= U_{i,t}^2 - 2\left(r_{ij}P_{ij,t} + x_{i,j}Q_{ij,t}\right) + \left(r_{ij}^2 + x_{ij}^2\right)I_{ij,t}^2 \\ P_{j,t}^{in} &= P_{ij,t} - r_{ij}I_{ij,t}^2 - \sum_{k:j\to k} P_{jk,t} \\ Q_{j,t}^{in} &= Q_{ij,t} - x_{ij}I_{ij,t}^2 - \sum_{k:j\to k} Q_{jk,t} \\ U_{i,t}^2 I_{ij,t}^2 &= P_{ij,t}^2 + Q_{ij,t}^2 \end{aligned} \tag{10}$$

where $U_{i,t}$ and $U_{j,t}$ are the voltage magnitudes of the corresponding nodes in time slot t. $P_{ij,t}$ and $Q_{ij,t}$ are the active and reactive power flowing from node i to node j on line ij in time slot t. $P_{j,t}^{in}$ and $Q_{j,t}^{in}$ are the active and reactive power injections at node j, respectively. $\sum_{k:j\to k} P_{jk,t}$ represents the sum of active power of all downstream branches starting from node j in time slot t, and $\sum_{k:j\to k} Q_{jk,t}$ represents the sum of reactive power of all downstream branches starting from node j in time slot t. x_{ij} and r_{ij} represent the reactance and resistance of line ij. $I_{ij,t}$ represents the current of line ij in time slot t. The system must satisfy the following operational constraints:

$$U_i^{\min} \le U_{i,t} \le U_i^{\max}, \left|I_{ij,t}\right| \le I_{ij}^{\max} \tag{11}$$

where $U_i^{\min}$ and $U_i^{\max}$ are the lower and upper limits of the voltage magnitude at node i, and $I_{ij}^{\max}$ is the maximum current limit for line ij, all of which are preset parameters.

Since the current-power relationship in the model, *i.e.*, $U_{i,t}^2 I_{ij,t}^2 = P_{ij,t}^2 + Q_{ij,t}^2$, is non-linear, it leads to non-convexity in the optimization problem, increasing the difficulty of solution. To obtain a convex optimization form, Second-Order Cone Programming (SOCP) is used to relax the aforementioned relationship. The relaxed problem is a convex problem, and using existing convex optimization algorithms guarantees finding the global optimal solution [37]. This SOCP relaxation is highly effective for radial distribution systems as it preserves the physical characteristics of the power flow while transforming the non-convex constraints into a computationally tractable form. Under most operational conditions, this relaxation is proven to be exact, ensuring that the optimal solution of the relaxed model

remains physically feasible for the original power network. Let $\mathcal{V}_{i,t} = U_{i,t}^2$ and $\mathcal{I}_{ij,t} = I_{ij,t}^2$. The relationship is relaxed to:

$$\left\| \begin{array}{c} 2P_{ij,t} \\ 2Q_{ij,t} \\ \mathcal{V}_{i,t} - \mathcal{I}_{ij,t} \end{array} \right\|_2 \le \mathcal{V}_{i,t} + \mathcal{I}_{ij,t} \tag{12}$$

In AC systems, power loss caused by resistance follows Joule's law and is proportional to the square of the current. The power loss of line ij in time slot t is:

$$P_{ij,t}^{Loss} = r_{ij} \cdot I_{ij,t}^2 \tag{13}$$

Then the transmission loss cost of line ij in time slot t is:

$$C_{ij,t}^{Loss} = \lambda_{ij,t}^{Loss} P_{ij,t}^{Loss} \tag{14}$$

where $\lambda_{ij,t}^{Loss}$ represents the cost coefficient for losses of line ij at time t.

3.2.2. Conventional Generation Cost

The cost of traditional thermal power generation units is commonly represented by a quadratic function. Let $P_{i_g,t}^G$ and $Q_{i_g,t}^G$ denote the active and reactive power output of the g-th generator at node i in time slot t, respectively. The following operational constraints must be satisfied:

$$\begin{aligned} & P_{i_g}^{G,\min} \le P_{i_g,t}^G \le P_{i_g}^{G,\max} \\ & Q_{i_g}^{G,\min} \le Q_{i_g,t}^G \le Q_{i_g}^{G,\max} \\ & \left| P_{i_g,t}^G - P_{i_g,t-1}^G \right| \le \Delta P_{i_g}^{G,\max} \\ & \left| Q_{i_g,t}^G - Q_{i_g,t-1}^G \right| \le \Delta Q_{i_g}^{G,\max} \end{aligned} \tag{15}$$

where $P_{i_g}^{G,\min}$, $P_{i_g}^{G,\max}$, $Q_{i_g}^{G,\min}$, and $Q_{i_g}^{G,\max}$ represent the minimum and maximum active and reactive power outputs of the g-th generation unit at node i, respectively. $\Delta P_{i_g}^{G,\max}$ and $\Delta Q_{i_g}^{G,\max}$ represent the maximum ramp rates in adjacent time slots.

The generation cost is only related to active power output, and reactive power output is not included in the main cost function. That is, the generation cost function of unit g in time slot t can be expressed as:

$$C_{i_g,t}^G = a_{i_g} \left(P_{i_g,t}^G \right)^2 + b_{i_g} P_{i_g,t}^G + c_{i_g} \tag{16}$$

where a_{i_g}, b_{i_g}, and c_{i_g} are the generation cost function coefficients for unit g, all of which are preset parameters.

3.2.3. Main Grid Power Purchase Cost

Distributed generation resources within the distribution network can satisfy local load demands to a certain extent, but their marginal generation costs typically rise with increased output. Therefore, under the condition of satisfying overall economic optimality, the PMSC can choose to purchase a portion of electricity from the upper-level main grid to better utilize the cost advantages of external resources

and achieve global economic dispatch. Assuming node 1 is the interconnection point between the distribution network and the main grid, the cost of purchasing electricity from the main grid can be expressed as:

$$C^T = \sum_{t=1}^{T} \lambda_t^{EX} P_{1,t}^{EX} \tag{17}$$

where $P_{1,t}^{EX}$ is the interaction power between the supply-side distribution network and the upper-level main grid, and λ_t^{EX} represents the electricity price provided by the upper-level main grid to the supply-side distribution network, which is a preset parameter.

3.2.4. Supply Side Welfare

The total welfare of the supply side is reflected as total electricity sales revenue minus total generation costs, transmission loss costs, and power purchase costs from the upper-level main grid. The congestion costs have already been reflected through the differences in nodal prices. To ensure the safe and stable operation of the power grid, real-time supply-demand balance and power flow constraints must be satisfied, as follows:

$$\begin{aligned} & P_{ij,t}^{\min} \le P_{ij,t} \le P_{ij,t}^{\max}, Q_{ij,t}^{\min} \le Q_{ij,t} \le Q_{ij,t}^{\max} \\ & P_{i,t}^{in} = -\sum_{g \in \boldsymbol{N}_i^G} P_{i_g,t}^G + P_{i,t}^L + \sum_{n \in \boldsymbol{N}_i^{MG}} P_{i_n,t}^{MG} \\ & Q_{i,t}^{in} = -\sum_{g \in \boldsymbol{N}_i^G} Q_{i_g,t}^G + Q_{i,t}^L + \sum_{n \in \boldsymbol{N}_i^{MG}} Q_{i_n,t}^{MG} \\ & Q_{i_n,t}^{MG} = \zeta \cdot P_{i_n,t}^{MG} \end{aligned} \tag{18}$$

where $P_{ij}^{\min}, P_{ij}^{\max}, Q_{ij}^{\min}, Q_{ij}^{\max}$ are the minimum and maximum active and reactive power allowed for line \$ij\$, which are all preset parameters. $P_{i,t}^{in}$ and $Q_{i,t}^{in}$ are the active and reactive power injections at node i, respectively. $Q_{i,t}^L$ is the total reactive power load at node i, and $Q_{i_n,t}^{MG}$ is the net reactive load of user i_n. To simplify the model, $Q_{i,t}^L$ is defined as a preset parameter, and ζ is a preset parameter representing the proportional relationship between net reactive power and net active power.

The total sales revenue and the corresponding price constraints are in the following form:

$$W = \sum_{i=1}^{N^B} \lambda_{i,t} \sum_{j \in \boldsymbol{N}_i^{MG}} P_{i_j,t}^{MG} \Delta t \tag{19}$$

The overall optimization objective of the supply side is to maximize total welfare:

$$C^{PS} = \sum_{t=1}^{T} \left(W - \sum_{i=1}^{N^B} \sum_{g \in \boldsymbol{N}_i^G} C_{i_g,t}^G - \sum_{ij \in N^L} C_{ij,t}^{Loss} - C^T \right) \tag{20}$$

where the first term is the total sales revenue, the second term is the total generation cost, the third term is the total loss cost, and the last term is the transaction cost with the main grid.

4. Model Solution

The pricing model constructed in this paper is a bi-level optimization problem. The upper-level supplier and lower-level user decisions are coupled, and the model includes non-convex power flow constraints and non-linear complementarity slackness conditions, making direct solution difficult. Therefore, this paper employs KKT conditions and strong duality theory to transform the lower-level problem into upper-level constraints. Furthermore, Second-Order Cone Programming (SOCP) relaxation and the Big-M method are used to handle power flow non-convexity and complementarity non-linearity, respectively, ultimately transforming the original problem into a Mixed-Integer Linear Programming (MILP) model that can be efficiently solved.

4.1. Upper-Level Problem: Supply Side Profit Maximization

The upper-level decision maker is the Power Market Scheduling Center (PMSC), which involves multiple nodes and generation units. It needs to formulate real-time nodal prices and supply plans to maximize its profit. This problem can be formulated as a non-linear programming model subject to various physical constraints (such as power balance and line capacity). The objective function comprehensively considers generation costs, electricity sales revenue, and network loss costs. Based on the system constraints and objective function described in the previous sections, the upper-level problem is formalized as:

$$\begin{aligned} &\max C^{PS} = \sum_{t=1}^{T}\left(W - \sum_{i=1}^{N^B}\sum_{g\in N_i^G} C_{i_g,t}^{G} - \sum_{ij\in N^L} C_{ij,t}^{Loss} - C^{T}\right) \\ &\text{s.t. (11) (12) (13) (14) (16) (19)} \end{aligned} \tag{21}$$

where the first term W is the total electricity sales revenue defined in Equation (19), the traditional thermal generation cost $C_{i_g,t}^{G}$ is defined in Equation (16), the distribution network loss cost $C_{ij,t}^{Loss}$ is defined in Equation (14), and the cost of purchasing power from the upper-level main grid C^{T} is defined in Equation (17).

4.2. Lower-Level Problem: User Welfare Maximization

The lower-level decision makers are the user groups, who maximize their welfare by adjusting electricity loads and energy storage operations. This problem is modeled as a convex quadratic programming model. Users respond to price signals by optimizing their consumption behavior and storage strategies. Based on the user load response constraints, the lower-level problem is formalized as:

$$\begin{aligned} &\min \sum_{t=1}^{T}\left(-U_{i_n,t}^{MG} + C_{i_n,t}^{RES} + C_{i_n,t}^{ESS} + C_{i_n,t}^{EX}\right) \\ &\text{s.t. (2) (3) (4) (6) (7)} \end{aligned} \tag{22}$$

where the user utility $U_{i_n,t}^{MG}$ is defined in Equation (1), the renewable energy equipment depreciation and maintenance cost $C_{i_n,t}^{RES}$ is defined in Equation (3), the energy storage charging/discharging cost $C_{i_n,t}^{ESS}$ is defined in Equation (5),

and the electricity purchase cost $C_{i_n,t}^{EX}$ is defined in Equation (8). In the lower-level problem, the depreciation and maintenance cost functions for renewable energy and storage devices are convex, and the utility function is concave; therefore, the lower-level problem (22) is a convex optimization problem.

4.3. KKT Conditions and Dual Optimization Transformation

To address the typical "upper-level maximization, lower-level minimization" structure of bi-level optimization, and to improve solution efficiency, KKT optimality conditions and duality theory are utilized to transform the original problem into an equivalent single-level mathematical programming problem. The specific steps are as follows:

4.3.1. Construction of Lagrangian Function for Lower-Level Problem

For the clarity of the solution process, the subsequent transformation targets a specific user under node i (subscripts regarding the user index are implicitly handled in the standard notation i_n). The Lagrangian function is constructed as:

$$\begin{aligned}
&L_i\left(P_{i,t}^L, P_{i,t}^{ESS}, P_{i,t}^{MG}\right) \\
&= \sum_{t=1}^{T}\Bigg(-\omega_{i,t}P_{i,t}^L + \frac{\alpha}{2}\left(P_{i,t}^L\right)^2 + \gamma_i^{RES}P_{i,t}^{RES} + \delta_i^{RES}\left(P_{i,t}^{RES}\right)^2 + \gamma_i^{ESS}P_{i,t}^{ESS} \\
&\quad + \delta_i^{ESS}\left(P_{i,t}^{ESS}\right)^2 + \lambda_{i,t}P_{i,t}^{MG}\Delta t\Bigg) - \sum_{t=1}^{T}\lambda_{i,t}^{ESS,\min}\left(P_{i,t}^{ESS} + P_i^{ESS,\max}\right) \\
&\quad - \sum_{t=1}^{T}\lambda_{i,t}^{ESS,\max}\left(P_i^{ESS,\max} - P_{i,t}^{ESS}\right) - \sum_{t=1}^{T}\lambda_{i,t}^{E,\min}\left(E_{i,0} + \sum_{\tau=1}^{t}\Delta t P_{i,\tau}^{ESS} - E_i^{\min}\right) \\
&\quad - \sum_{t=1}^{T}\lambda_{i,t}^{E,\max}\left(E_i^{\max} - E_{i,0} - \sum_{\tau=1}^{t}\Delta t P_{i,\tau}^{ESS}\right) - \sum_{t=1}^{T}\lambda_{i,t}^{MG,\min}P_{i,t}^{MG} \\
&\quad - \sum_{t=1}^{T}\lambda_{i,t}^{L,\min}\left(P_{i,t}^L - P_i^{L,\min}\right) - \sum_{t=1}^{T}\lambda_{i,t}^{L,\max}\left(P_i^{L,\max} - P_{i,t}^L\right) \\
&\quad + \mu_i^E\sum_{t=1}^{T}\Delta t P_{i,t}^{ESS} + \sum_{t=1}^{T}\mu_{i,t}^{eq}\left(P_{i,t}^{MG} - P_{i,t}^{ESS} - P_{i,t}^L + P_{i,t}^{RES}\right)
\end{aligned} \tag{23}$$

4.3.2. KKT Conditions

Since the lower-level problem is a convex quadratic programming problem and satisfies Slater's constraint qualification, its optimal solution must satisfy the KKT necessary and sufficient conditions.

$$\begin{aligned}
&\forall t \in \{1, T\}: \\
&\frac{\partial L_i}{\partial P_{i,t}^{ESS}} = \gamma_i^{ESS} + 2\delta_i^{ESS}P_{i,t}^{ESS} - \lambda_{i,t}^{ESS,\min} + \lambda_{i,t}^{ESS,\max} \\
&\qquad + \Delta t\sum_{\tau=t}^{T}\left(\lambda_{i,\tau}^{E,\max} - \lambda_{i,\tau}^{E,\min}\right) + \mu_i^E\Delta t - \mu_{i,t}^{eq} = 0, \\
&\frac{\partial L_i}{\partial P_{i,t}^{MG}} = \lambda_{i,t}\Delta t - \lambda_{i,t}^{MG,\min} + \mu_{i,t}^{eq} = 0, \\
&\frac{\partial L_i}{\partial P_{i,t}^{L}} = -\omega_{i,t} + \alpha P_{i,t}^L - \lambda_{i,t}^{L,\min} + \lambda_{i,t}^{L,\max} - \mu_{i,t}^{eq} = 0
\end{aligned}$$

$$\begin{aligned}
&\lambda_{i,t}^{ESS,\max}\left(P_i^{ESS,\max}-P_{i,t}^{ESS}\right)=0,\lambda_{i,t}^{ESS,\min}\left(P_{i,t}^{ESS}+P_i^{ESS,\max}\right)=0,\\
&\lambda_{i,t}^{E,\min}\left(E_{i,0}+\sum_{\tau=1}^{t}\Delta tP_{i,\tau}^{ESS}-E_i^{\min}\right)=0,\lambda_{i,t}^{E,\max}\left(E_i^{\max}-E_{i,0}-\sum_{\tau=1}^{t}\Delta tP_{i,\tau}^{ESS}\right)=0,\\
&\lambda_{i,t}^{L,\min}\left(P_{i,t}^{L}-P_i^{L,\min}\right)=0,\lambda_{i,t}^{L,\max}\left(P_i^{L,\max}-P_{i,t}^{L}\right)=0,\\
&\lambda_{i,t}^{MG,\min}P_{i,t}^{MG}=0\\
&\lambda_{i,t}^{ESS,\min},\lambda_{i,t}^{ESS,\max},\lambda_{i,t}^{E,\max},\lambda_{i,t}^{E,\min},\lambda_{i,t}^{RES\min},\lambda_{i,t}^{RES\max},\lambda_{i,t}^{MG,\min}\geq 0,
\end{aligned}\tag{24}$$

4.3.3. Linearization of Non-Linear Constraints

For the complementary slackness terms in the KKT conditions in the form of $x\cdot y=0$, $(x,y\geq 0)$, the Big-M method is employed for linearization. A binary variable $\theta\in\{0,1\}$ and a sufficiently large positive real number M are introduced to construct the equivalent constraints:

$$\begin{aligned}
&0\leq x\leq M\theta\\
&0\leq y\leq M(1-\theta)
\end{aligned}\tag{25}$$

When $\theta=1$, $0\leq x\leq M$ and $y=0$; when $\theta=0$, $x=0$ and $0\leq y\leq M$. Thus, the linearization transformation of the non-linear terms is achieved.

4.3.4. Application of Strong Duality Theorem

Based on the strong duality theorem, the optimal solution of the lower-level problem can be equivalently described by its dual problem. The equivalent expression for the optimal solution of the lower-level problem derived from the strong duality theorem is:

$$\begin{aligned}
&\sum_{t=1}^{T}\left(-\omega_{i,t}P_{i,t}^{L}+\frac{\alpha}{2}\left(P_{i,t}^{L}\right)^2+\gamma_i^{RES}P_{i,t}^{RES}+\delta_i^{RES}\left(P_{i,t}^{RES}\right)^2\right.\\
&\left.+\gamma_i^{ESS}P_{i,t}^{ESS}+\delta_i^{ESS}\left(P_{i,t}^{ESS}\right)^2+\lambda_{i,t}P_{i,t}^{MG}\Delta t\right)\\
&=\gamma_i^{RES}P_{i,t}^{RES}+\delta_i^{RES}\left(P_{i,t}^{RES}\right)^2-P_i^{ESS,\max}\sum_{t=1}^{T}\lambda_{i,t}^{ESS,\min}-P_i^{ESS,\max}\sum_{t=1}^{T}\lambda_{i,t}^{ESS,\max}\\
&-\left(E_{i,0}-E_i^{\min}\right)\sum_{t=1}^{T}\lambda_{i,t}^{E,\min}-\left(E_i^{\max}-E_{i,0}\right)\sum_{i=1}^{T}\lambda_{i,t}^{E,\max}+\sum_{t=1}^{T}\lambda_{i,t}^{L,\min}P_i^{L,\min}\\
&-\sum_{t=1}^{T}\lambda_{i,t}^{L,\max}P_i^{L,\max}+\sum_{t=1}^{T}\mu_{i,t}^{eq}P_{i,t}^{RES}
\end{aligned}\tag{26}$$

In summary, after substituting the KKT conditions into the upper-level problem, the master-slave game model can be transformed into the following Mixed-Integer Linear Programming (MILP) problem:

$$\max C^{PS}=\sum_{i=1}^{N^B}\sum_{n\in N_i^{MG}}\left(C_{i_n,1}-C_{i_n,2}\right)+\sum_{t=1}^{T}\left(-\sum_{i=1}^{N^B}\sum_{g\in N_i^{G}}C_{i_g,t}^{G}-\sum_{ij\in N^L}C_{ij,t}^{Loss}-C^{T}\right)$$

$$\begin{aligned}
\text{s.t. } C_{i_n,1}=&-P_i^{ESS,\max}\sum_{t=1}^{T}\lambda_{i,t}^{\mathrm{ESS,min}}-P_i^{ESS,\max}\sum_{t=1}^{T}\lambda_{i,t}^{\mathrm{ESS,max}}\\
&-\left(E_{i,0}-E_i^{\min}\right)\sum_{t=1}^{T}\lambda_{i,t}^{\mathrm{E,min}}-\left(E_i^{\max}-E_{i,0}\right)\sum_{i=1}^{T}\lambda_{i,t}^{\mathrm{E,max}}\\
&+\sum_{t=1}^{T}\lambda_{i,t}^{\mathrm{L,min}}P_i^{L,\min}-\sum_{t=1}^{T}\lambda_{i,t}^{\mathrm{L,max}}P_i^{L,\max}+\sum_{t=1}^{T}\mu_{i,t}^{eq}P_{i,t}^{RES}
\end{aligned}$$

$$C_{i_n,2} = \sum_{t=1}^{T}\left(-\omega_{i,t}P_{i,t}^{L} + \frac{\alpha}{2}\left(P_{i,t}^{L}\right)^2 + \gamma_i^{ESS}P_{i,t}^{ESS} + \delta_i^{ESS}\left(P_{i,t}^{ESS}\right)^2\right) \quad (27)$$

s.t. (11) (12) (13) (14) (16) (19)

This problem belongs to the class of mixed-integer linear programming problems and can be efficiently solved using commercial solvers.

5. Simulation Experiment

Simulation experiments are conducted on a power grid system comprising both the supply side and the demand side to validate the effectiveness of the proposed model. The supply side includes distributed small-scale generator sets and interfaces for purchasing electricity from the upper-level main grid, while the demand side consists of multiple small-scale microgrids. A modified IEEE 33-bus distribution system is employed for the simulation. Specific modifications include: removing the fixed loads of the original system to highlight the regulatory role of demand-side resources; and proportionally scaling down line impedance. This modification is necessary to reflect the shorter physical distances and lower voltage drops characteristic of small-scale residential microgrids compared to standard medium-voltage distribution feeders, thereby ensuring the simulation results are representative of a localized energy community environment.

5.1. Simulation Setup

The structure of the simulation system is shown in **Figure 1**. The supply side consists of two parts: first, small-scale thermal power generating units deployed at nodes 6, 8, and 13 of the distribution network; second, electricity trading with the upper-level main grid via the connection at node 1. The demand side includes three independent microgrids located at nodes 8, 18, and 33, with each microgrid containing three residential users. Each user is equipped with photovoltaic (PV) generation equipment, wind power generation equipment, and a home energy storage system. The scheduling period is set to one day, divided into 24 equal time slots ($t = 1, 2, \cdots, 24$). The cost function of the generator sets is defined by Equation (16), and the relevant parameters are listed in **Table 1**.

Table 1. Relevant parameters of generator sets.

Unit No	Capacity (kW)	Min Output (kW)	a (CNY/kW²h)	b (CNY/kWh)	c (CNY/h)
unit1	150	40	0.0035	0.380	2
unit2	120	20	0.0042	0.290	2
unit3	90	15	0.0046	0.393	1

The user electricity utility function is defined as Equation (1), where $\omega \in [1,5]$ takes random values and $\alpha = 0.1$. The parameter ω for different users takes different values in different time slots. The total capacity of solar PV and wind power generation equipment installed by each user is 10 kW, and the capacity of

the energy storage equipment is 10 kWh. Figure 2 depicts the output of solar PV and wind power generation within a day based on statistical characteristics. Although the marginal cost of renewable energy generation is zero, equipment maintenance and depreciation costs must still be considered. The parameters are set as $\gamma_{i_n}^{RES} = \gamma_{i_n}^{ESS} = 0$ and $\delta_{i_n}^{RES} = \delta_{i_n}^{ESS} = 0.01$. The wholesale electricity price released by the main grid is known, and its price curve is visible in Figure 3. The real-time electricity price released by the PMSC is required to fluctuate within a certain range: the lower limit is set at 0.8 times the main grid benchmark price, and the upper limit is set at 3 times. Additionally, $\zeta = 0.5$, assuming that the net reactive power is 0.5 times the net active power.

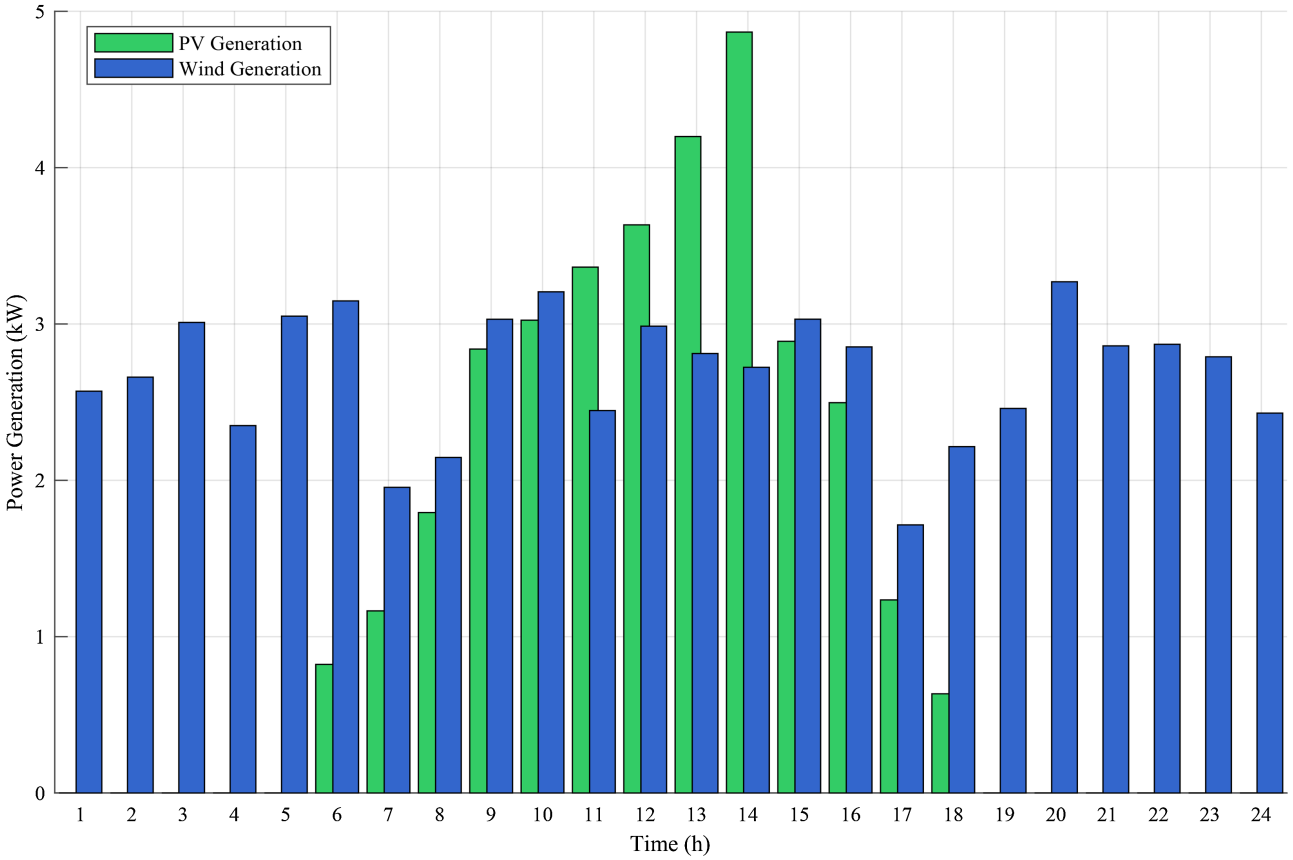

Figure 2. Solar and wind power output of user 3.

5.2. Result Analysis

Based on the parameter settings mentioned above, Figure 3 illustrates the optimal electricity prices for each microgrid under the proposed real-time locational marginal pricing strategy, alongside the benchmark price of the upper-level main grid. Figure 4 presents the optimal dispatch scheme for the system's total consumption, total supply, renewable energy, and energy storage. As depicted in Figure 4, the total consumption by users exceeds the total supply, indicating that users utilized power generated from their own renewable energy sources or discharged from energy storage devices. In fact, by adhering to constraint (6), the

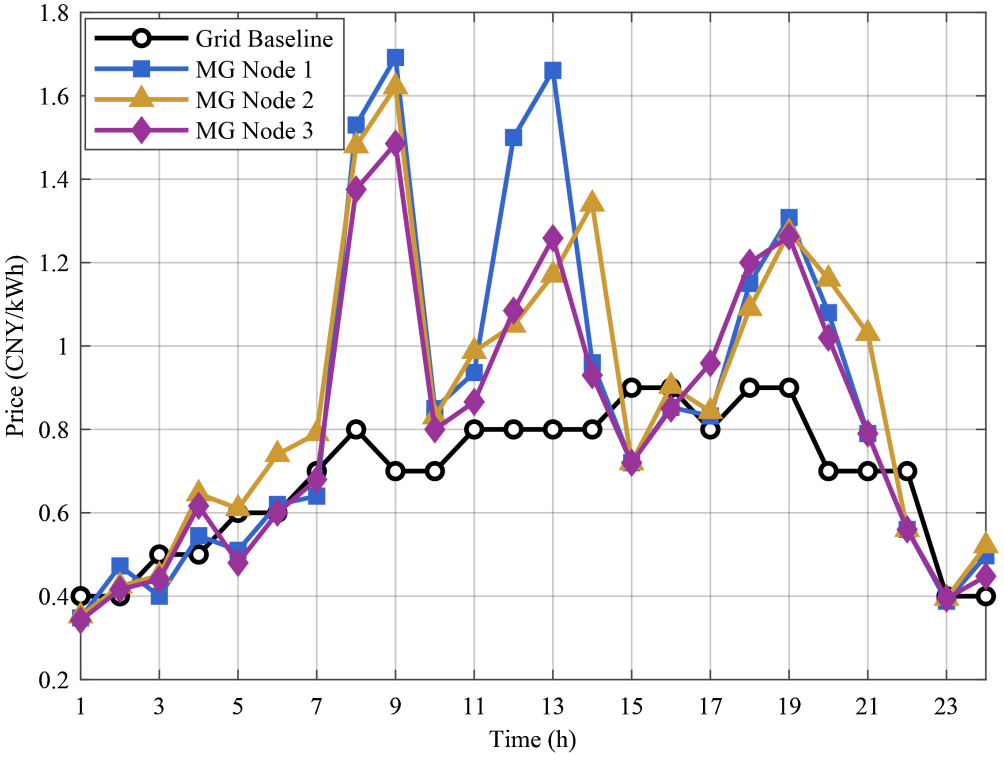

Figure 3. Time-series comparison of nodal real-time electricity prices in the microgrid and the benchmark main grid prices.

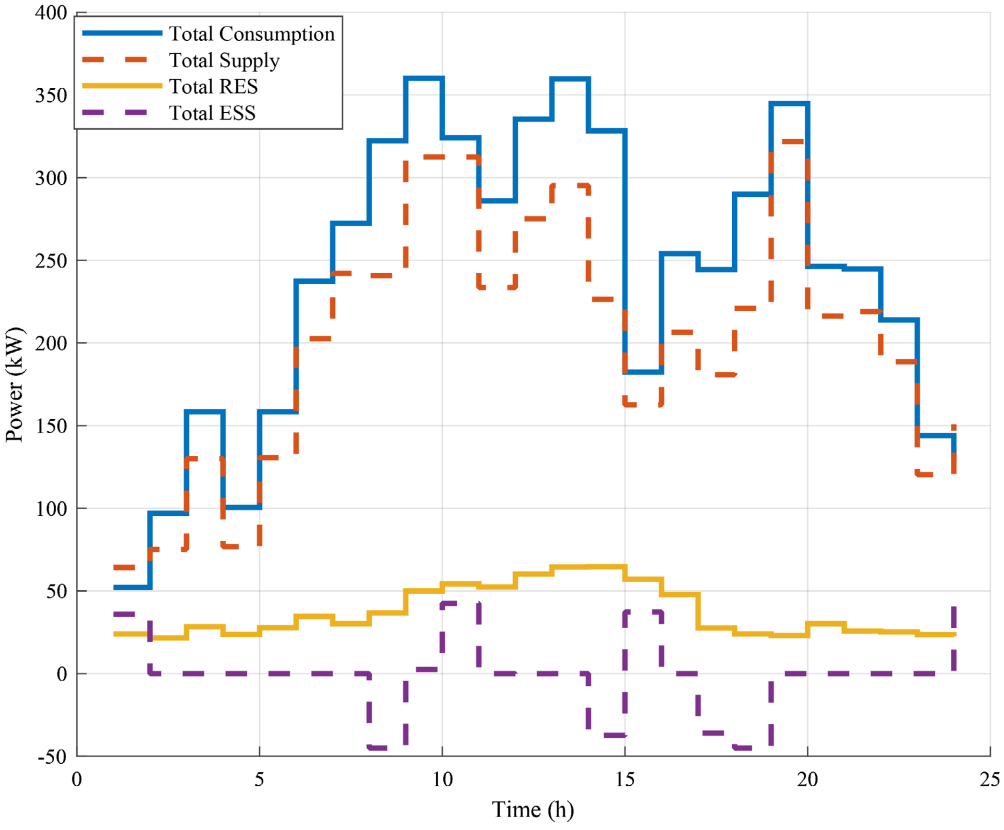

Figure 4. Time-series variation of system power balance.

balance between the supply side and the demand side is strictly maintained. Taking User 3 as an example, Figure 5 displays the optimal energy dispatch scheme on the demand side over the operation cycle, covering electricity consumption, renewable energy output, and charging/discharging energy. Figure 6 illustrates the optimal power supply dispatch on the supply side.

Based on Figures 3-6, it can be concluded that throughout the scheduling cycle, electricity price fluctuations are correlated with user consumption preferences, renewable energy production, the benchmark price of the upper-level main grid, and the total cost of generation units. During periods with lower energy consumption and lower main grid prices, such as time slots 1 - 6 and 22 - 24, or periods with higher renewable energy output, such as time slots 10 - 14, electricity prices are relatively low. Conversely, during periods of high energy consumption and high main grid prices, such as time slots 9 - 10 and 19 - 21, electricity prices are relatively high, indicating that users actively participate in electricity market regulation. Furthermore, differences in the amplitude of price fluctuations exist among different microgrids, which primarily stem from three factors: first, there are differences in electricity consumption preferences among users in different microgrids; second, generation costs vary for units at different locations in the distribution system, allowing nodes located near low-cost power sources to prioritize the utilization of more economical power resources; third, nodal prices are also influenced by line transmission distances and network losses. In the proposed

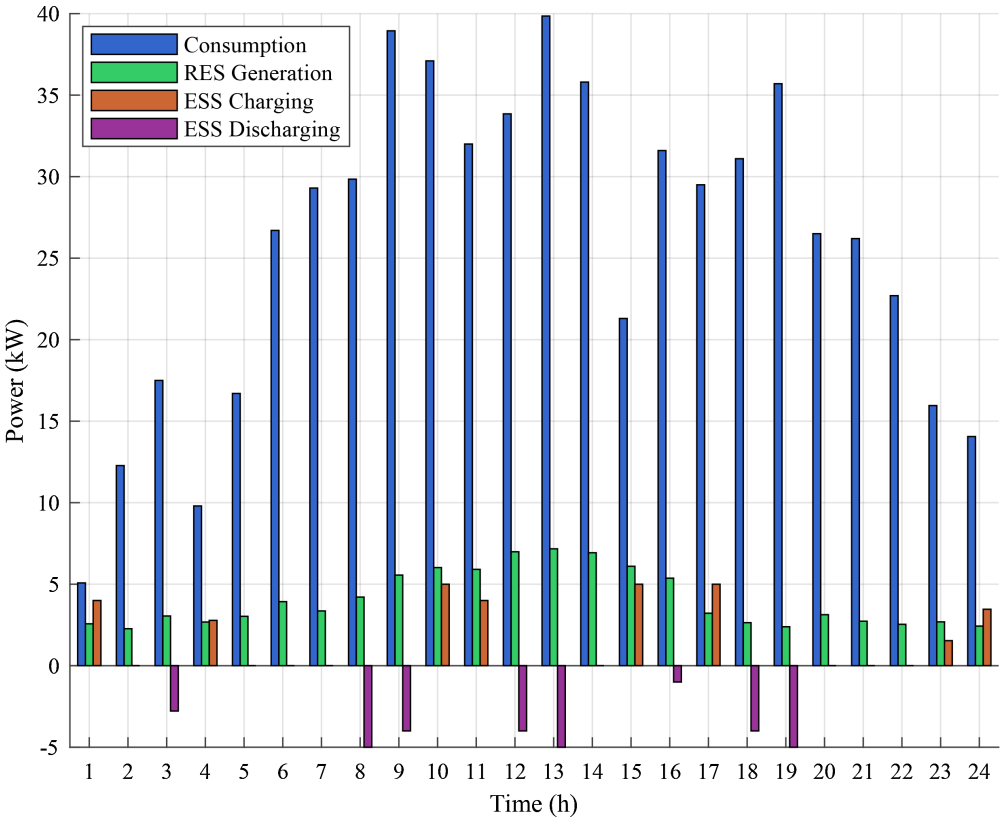

Figure 5. Electricity dispatch curve for user 3 at the microgrid node.

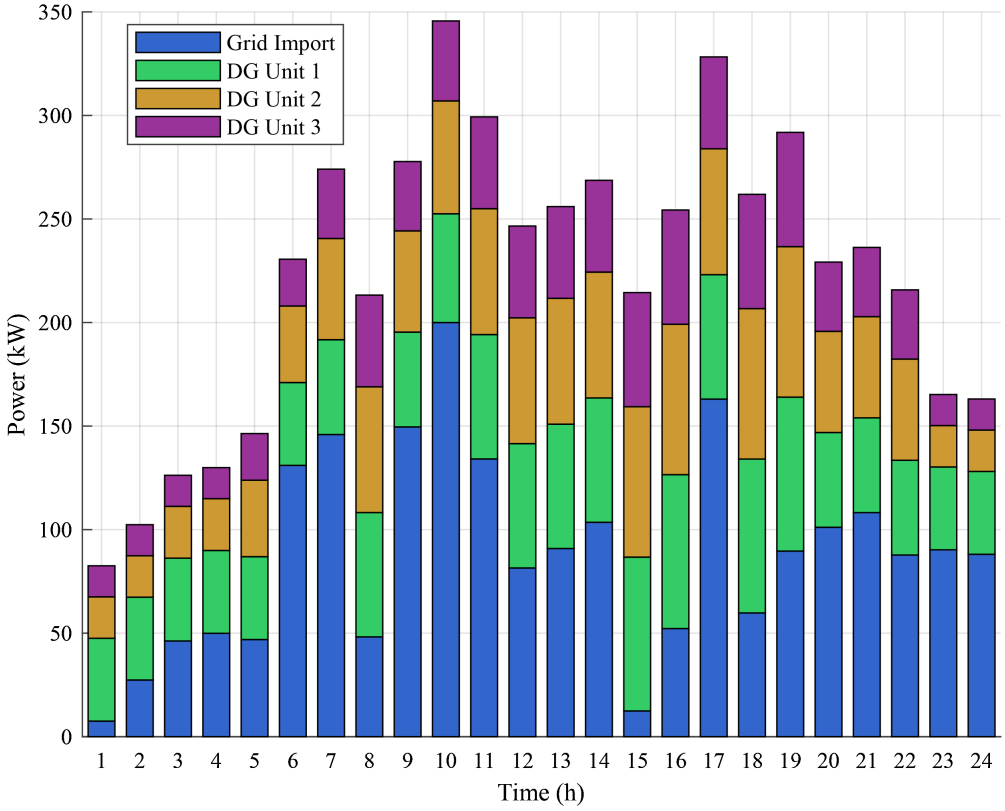

Figure 6. Optimal supply-side dispatch scheme.

model, the LMP is decomposed into marginal generation cost and marginal loss cost. By solving the dual variables of the power flow constraints (10)-(12), the mechanism specifically quantifies the additional cost required to supply an incremental unit of load at a specific node while accounting for the corresponding increase in system-wide ohmic losses, which is then directly integrated into the final nodal price.

5.3. Comparison of Different Renewable Energy Output Scenarios

To verify the effectiveness and robustness of our model, operational results are compared under two different renewable energy configuration ratios. As described in Section 4.1, in Scenario (a), users are equipped with 5 kW photovoltaic (PV) and wind power generation equipment, whereas in Scenario (b), the installed capacity of both types of renewable energy equipment is increased to 10 kW. The simulation assumptions and parameter settings remain consistent across both scenarios. Figure 7 illustrates the PV and wind power output over a single day under Scenario (b).

To conduct an in-depth analysis of the impact of increased renewable energy penetration on grid operation and the interaction mechanism between supply and demand, a comparative analysis is performed from the perspective of multiple indicators. Figure 8 displays the optimized energy dispatch scheme for User 3 in Scenario (b). Compared with Scenario (a), the user's optimal consumption plan

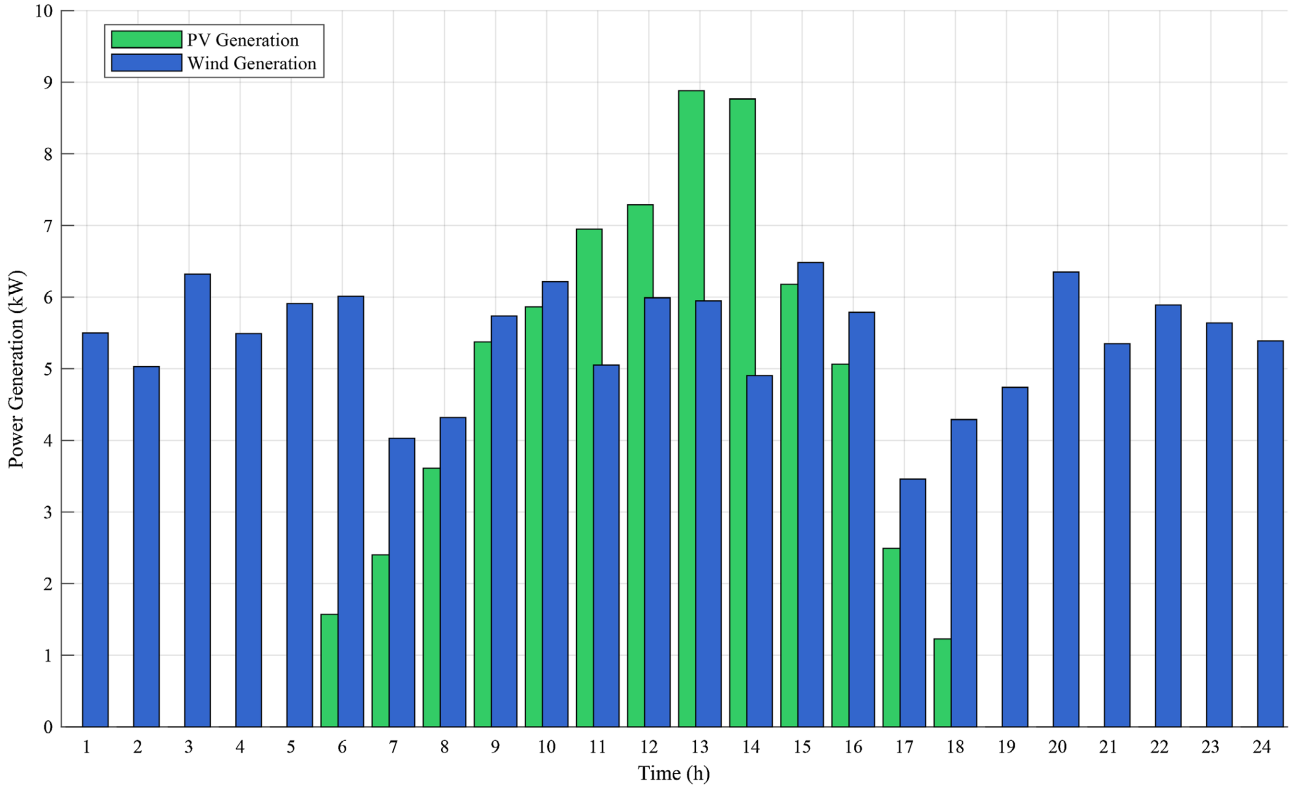

Figure 7. Solar and wind power output of user 3 in Scenario B.

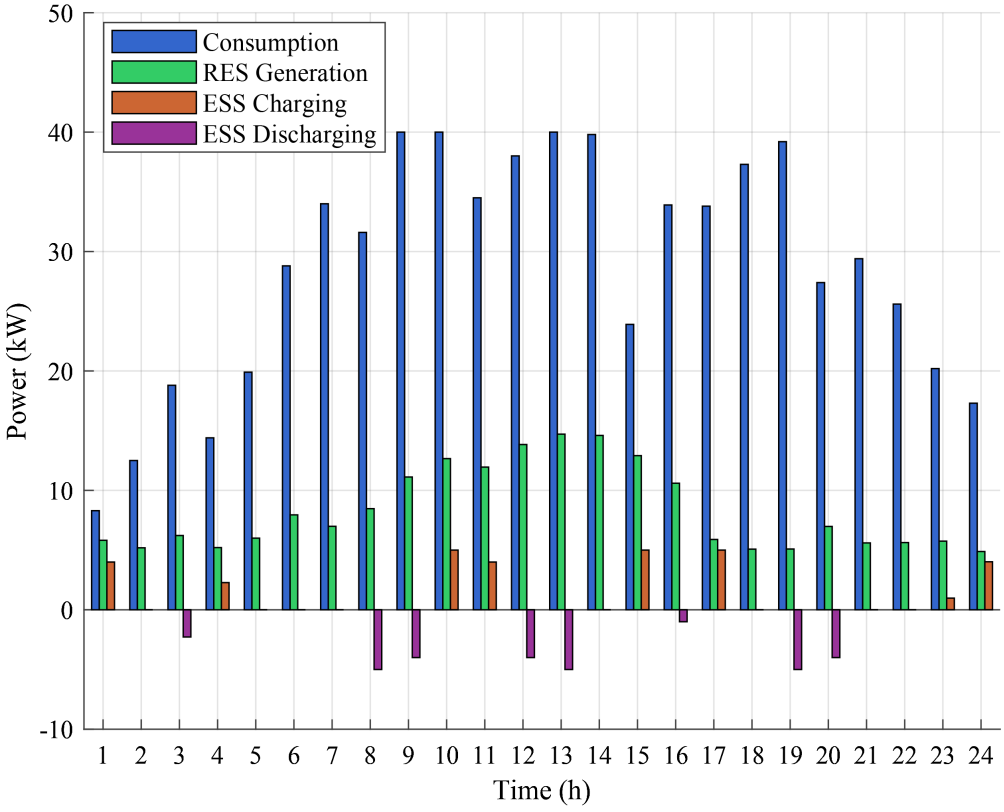

Figure 8. Electricity dispatch curve for user 3 at the microgrid node in scenario B.

remains substantially consistent, primarily due to the similarity in load characteristics and daily consumption patterns between the two scenarios. However, as the installed capacity of renewable energy increases, the proportion of electricity purchased from the grid significantly decreases, indicating a greater tendency for users to utilize local renewable energy to satisfy their own power demands. Based on the analysis of the supply-demand interaction mechanism, the PMSC adopts a strategy of reducing generation to achieve supply-demand balance in this situation. As shown in Figure 9, the optimal supply-side dispatch scheme in this scenario corroborates this observation.

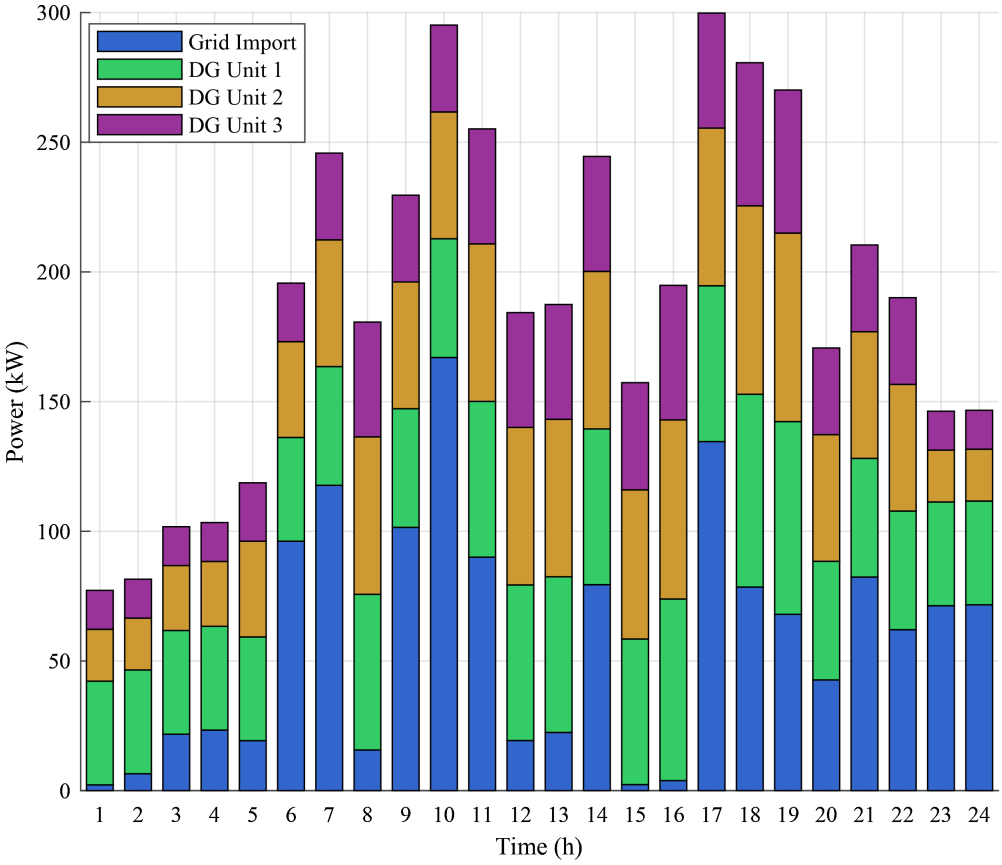

Figure 9. Optimal supply-side dispatch scheme under scenario B.

Particularly during daytime periods with abundant solar energy, the output of traditional generators exhibits a significant decline. This indicates that in power systems with a high proportion of renewable energy, characteristics such as the intermittency and volatility of renewable energy output exert a more pronounced inhibitory effect on the generation schedules of thermal units. Additionally, Figure 10 compares the social welfare levels under the two scenarios. The results show that social welfare in Scenario (b) is higher than that in Scenario (a), primarily attributed to the lower generation costs of renewable energy. This result not only confirms the significant value of renewable energy in enhancing the economic efficiency and sustainability of power systems but also validates the

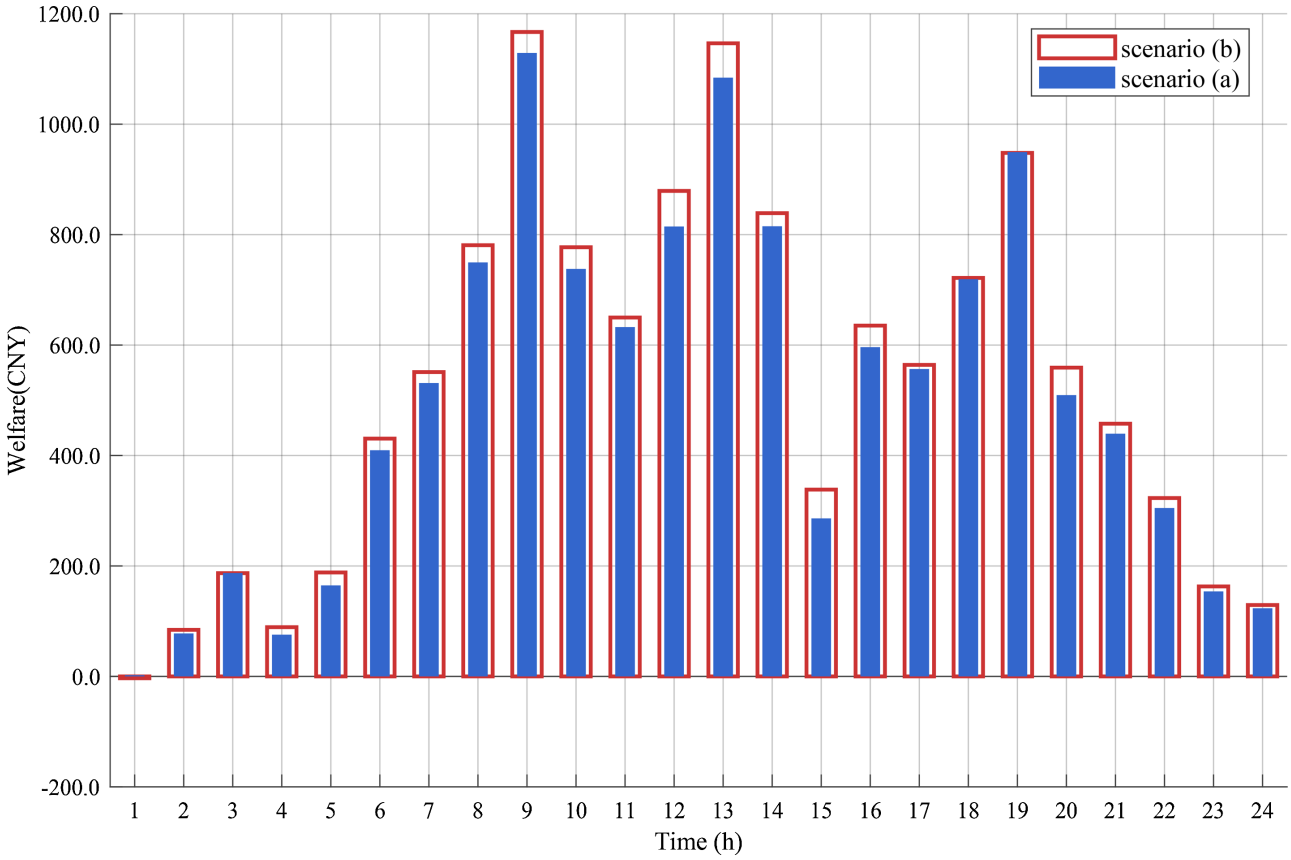

Figure 10. Social welfare in Scenario A vs. Scenario B.

effectiveness of the proposed pricing mechanism in environments with high renewable energy integration. The mechanism helps incentivize the accommodation and development of renewable energy, thereby reducing dependence on traditional fossil fuels and promoting the reduction of carbon emissions in system operation.

5.4. Result Analysis under Different Pricing Mechanisms

To evaluate the performance of the proposed pricing mechanism, this subsection compares the proposed real-time locational marginal pricing mechanism with the traditional fixed pricing mechanism [17] under consistent simulation conditions.

Figure 11 illustrates the hourly variations in social welfare under the two mechanisms throughout the full operation cycle. The results indicate that the real-time locational marginal price achieved a total social welfare of 12039.97 CNY, representing an increase of 9.45% compared to 10999.96 CNY under the fixed pricing mechanism. This demonstrates that real-time locational pricing possesses significant advantages in enhancing the overall economic efficiency of the system.

6. Conclusions

Against the background of high-penetration renewable energy integration into the grid, this study constructs a bi-level optimization framework considering

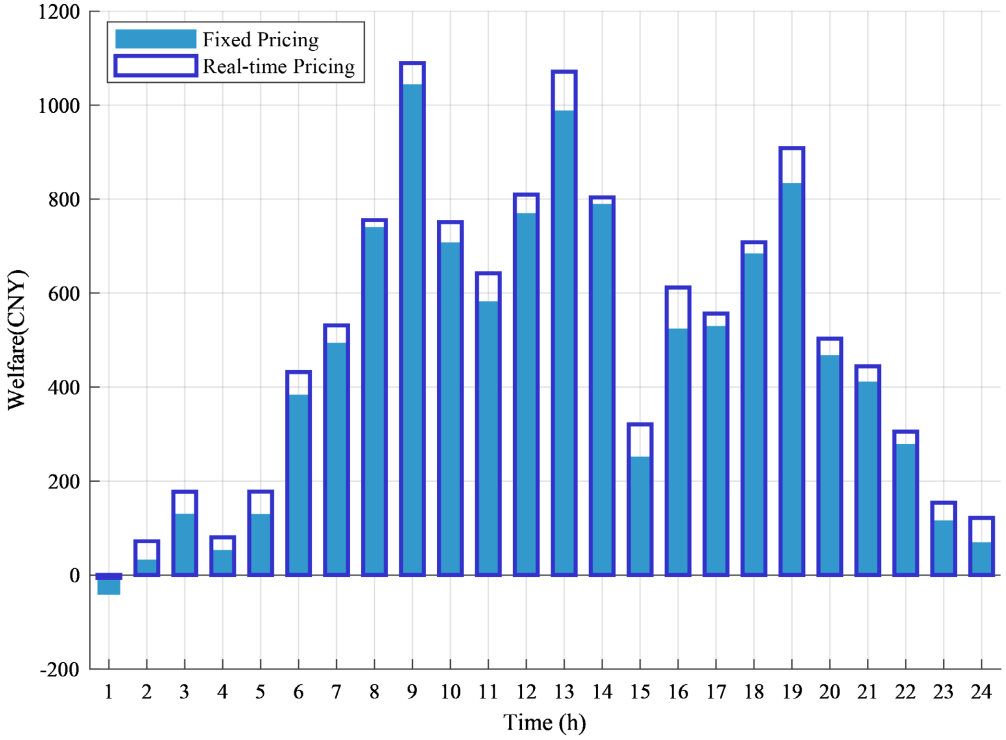

Figure 11. Social welfare values under the two mechanisms.

power flow physical constraints, successfully designing and verifying a locational marginal real-time pricing mechanism that balances economic efficiency and operational safety. In terms of modeling integrity, it addresses the limitations of traditional RTP and LMP, providing a feasible new approach for grid pricing under high renewable energy penetration. Theoretically, by constructing a Stackelberg game framework and employing the DistFlow power flow model with Second-Order Cone Programming (SOCP) relaxation techniques, the original problem is transformed into an efficiently solvable Mixed-Integer Linear Programming (MILP) problem, ensuring the rigor and practicality of the model. On the application level, simulation results based on a modified IEEE 33-node system demonstrate that the proposed mechanism can effectively guide demand-side users to adjust consumption behaviors and promote local accommodation of renewable energy, thereby reducing dependence on traditional fossil fuels and decreasing carbon emissions. Comparisons under different renewable energy penetration scenarios further validate that this pricing mechanism yields significant effects in enhancing total social welfare and improving system operational efficiency, offering effective theoretical methods and decision support for the economic, reliable, and low-carbon operation of power systems with high renewable energy shares.

Room for further expansion remains in this study. For instance, the uncertainty of renewable energy output could be addressed by introducing stochastic optimization or robust optimization methods; user behavior models could also be refined with actual data to improve response prediction accuracy. Additionally, future work could explore pricing strategies across multiple time scales to better

adapt to real-time scheduling and market trading demands. However, the practical implementation of this advanced LMP strategy may face challenges such as the need for high-granularity metering infrastructure and the requirement for robust communication low-latency to support real-time demand response.

Conflicts of Interest

The authors declare no conflicts of interest regarding the publication of this paper.

References

[1] Grigsby, L.L. (2012) Power System Stability and Control. 3rd Edition, CRC Press.

[2] He, Y., Gu, C., Gao, Y. and Wang, J. (2025) Bi-Level Day-Ahead and Real-Time Hybrid Pricing Model and Its Reinforcement Learning Method. *Energy*, **322**, Article 135316. https://doi.org/10.1016/j.energy.2025.135316

[3] Zhang, D., Han, R., Wan, Y., Qin, J., Ran, L. and Ma, Q. (2023) Robust Optimal Energy Management with Dynamic Price Response: A Non-Cooperative Multi-Community Aggregative Game Perspective. *International Journal of Electrical Power & Energy Systems*, **154**, Article 109395. https://doi.org/10.1016/j.ijepes.2023.109395

[4] Albogamy, F.R., Ashfaq, Y., Hafeez, G., Murawwat, S., Khan, S., Ali, F., *et al.* (2022) Optimal Demand-Side Management Using Flat Pricing Scheme in Smart Grid. *Processes*, **10**, Article 1214. https://doi.org/10.3390/pr10061214

[5] Dey, B., Misra, S. and Garcia Marquez, F.P. (2023) Microgrid System Energy Management with Demand Response Program for Clean and Economical Operation. *Applied Energy*, **334**, Article 120717. https://doi.org/10.1016/j.apenergy.2023.120717

[6] Khan, F.A., Ullah, K., Ur Rahman, A. and Anwar, S. (2023) Energy Optimization in Smart Urban Buildings Using Bio-Inspired Ant Colony Optimization. *Soft Computing*, **27**, 973-989. https://doi.org/10.1007/s00500-022-07537-3

[7] Kim, I. and Kim, W. (2023) Application of Market-Based Control with Thermal Energy Storage System for Demand Limiting and Real-Time Pricing Control. *Energy*, **263**, Article 125579. https://doi.org/10.1016/j.energy.2022.125579

[8] Gao, Y. (2020) Research on Social Welfare Maximization Model of Real-Time Pricing in Smart Grid. *Chinese Journal of Management Science*, **28**, 201-209.

[9] Li, N. and Gao, Y. (2023) Real-Time Pricing Based on Convex Hull Method for Smart Grid with Multiple Generating Units. *Energy*, **285**, Article 129543. https://doi.org/10.1016/j.energy.2023.129543

[10] Zhu, H., Gao, Y., Hou, Y., Wang, Z. and Feng, X. (2019) Real-Time Pricing Considering Different Type of Smart Home Appliances Based on Markov Decision Process. *International Journal of Electrical Power & Energy Systems*, **107**, 486-495. https://doi.org/10.1016/j.ijepes.2018.12.002

[11] Lyu, C., Jia, Y. and Xu, Z. (2021) Fully Decentralized Peer-to-Peer Energy Sharing Framework for Smart Buildings with Local Battery System and Aggregated Electric Vehicles. *Applied Energy*, **299**, Article 117243. https://doi.org/10.1016/j.apenergy.2021.117243

[12] Qu, D., Li, J. and Wang, X. (2025) Real-Time Pricing Strategy for Smart Grid Based on Game Analysis. *Systems Engineering-Theory & Practice*, **45**, 974-984.

[13] Zhu, Z., Gao, Y. and Ding, X. (2024) Two-Period Integrated Pricing Strategy for Smart Grid Based on Demand Side Management. *Chinese Journal of Management*

Science.

[14] Li, J., Zhang, T., Qu, D. and Pan, L. (2022) Real-Time Pricing of Smart Grid Based on Blockchain Privacy Protection. *Journal of University of Shanghai for Science and Technology*, **44**, 122-130.

[15] Caramanis, M., Bohn, R. and Schweppe, F. (1982) Optimal Spot Pricing: Practice and Theory. *IEEE Transactions on Power Apparatus and Systems*, **101**, 3234-3245. https://doi.org/10.1109/tpas.1982.317507

[16] Gao, Y. (2022) Review of Real-Time Pricing Optimization Methods Based on Demand Side Management. *Journal of University of Shanghai for Science and Technology*, **44**, 103-111, 121.

[17] Samadi, P., Mohsenian-Rad, A., Schober, R., Wong, V.W.S. and Jatskevich, J. (2010) Optimal Real-Time Pricing Algorithm Based on Utility Maximization for Smart Grid. 2010 *First IEEE International Conference on Smart Grid Communications*, Gaithersburg, 4-6 October 2010, 415-420. https://doi.org/10.1109/smartgrid.2010.5622077

[18] Yang, Y., Du, S. and Chen, Y. (2023) Real-Time Pricing Method for Smart Grid Based on Social Welfare Maximization Model. *Journal of Industrial and Management Optimization*, **19**, 2206-2225. https://doi.org/10.3934/jimo.2022039

[19] Li, Y., Li, J., Yu, Z., Dong, J. and Zhou, T. (2022) A Cosh-Based Smoothing Newton Algorithm for the Real-Time Pricing Problem in Smart Grid. *International Journal of Electrical Power & Energy Systems*, **135**, Article 107296. https://doi.org/10.1016/j.ijepes.2021.107296

[20] Umer, K., Huang, Q., Khorasany, M., Afzal, M. and Amin, W. (2021) A Novel Communication Efficient Peer-to-Peer Energy Trading Scheme for Enhanced Privacy in Microgrids. *Applied Energy*, **296**, Article 117075. https://doi.org/10.1016/j.apenergy.2021.117075

[21] van Leeuwen, G., AlSkaif, T., Gibescu, M. and van Sark, W. (2020) An Integrated Blockchain-Based Energy Management Platform with Bilateral Trading for Microgrid Communities. *Applied Energy*, **263**, Article 114613. https://doi.org/10.1016/j.apenergy.2020.114613

[22] Zhang, L., Gao, Y., Zhu, H. and Tao, L. (2022) Bi-Level Stochastic Real-Time Pricing Model in Multi-Energy Generation System: A Reinforcement Learning Approach. *Energy*, **239**, Article 121926. https://doi.org/10.1016/j.energy.2021.121926

[23] Zhang, L., Gao, Y., Zhu, H. and Tao, L. (2022) A Distributed Real-Time Pricing Strategy Based on Reinforcement Learning Approach for Smart Grid. *Expert Systems with Applications*, **191**, Article 116285. https://doi.org/10.1016/j.eswa.2021.116285

[24] Luo, Y., Gao, Y. and Fan, D. (2023) Real-Time Demand Response Strategy Base on Price and Incentive Considering Multi-Energy in Smart Grid: A Bi-Level Optimization Method. *International Journal of Electrical Power & Energy Systems*, **153**, Article 109354. https://doi.org/10.1016/j.ijepes.2023.109354

[25] Tao, L., Gao, Y., Liu, Y. and Zhu, H. (2020) A Rolling Penalty Function Algorithm of Real-Time Pricing for Smart Microgrids Based on Bilevel Programming. *Engineering Optimization*, **52**, 1295-1312. https://doi.org/10.1080/0305215x.2019.1642882

[26] Pandey, V.C., Rawat, T., Ospina, J., Dvorkin, Y. and Konstantinou, C. (2025) A Tri-Level Distribution Locational Marginal Price-Based Demand Response Framework. *Electric Power Systems Research*, **241**, Article 111398. https://doi.org/10.1016/j.epsr.2024.111398

[27] Bai, L., Wang, J., Wang, C., Chen, C. and Li, F. (2018) Distribution Locational Mar-

ginal Pricing (DLMP) for Congestion Management and Voltage Support. *IEEE Transactions on Power Systems*, **33**, 4061-4073. https://doi.org/10.1109/tpwrs.2017.2767632

[28] Wang, X., Gao, F., Kang, C., Li, C., Liu, Q., Han, Y., *et al.* (2019) Research on Extended Nodal Pricing Algorithm. *Power System Technology*, **43**, 3587-3596.

[29] Liu, H., Guo, Y. and Sun, H. (2022) Review and Prospect of Inter-Regional and Inter-Provincial Power Trading in China. *Automation of Electric Power Systems*, **46**, 187-199.

[30] Haider, R., D'Achiardi, D., Venkataramanan, V., Srivastava, A., Bose, A. and Annaswamy, A.M. (2021) Reinventing the Utility for Distributed Energy Resources: A Proposal for Retail Electricity Markets. *Advances in Applied Energy*, **2**, Article 100026. https://doi.org/10.1016/j.adapen.2021.100026

[31] Mieth, R. and Dvorkin, Y. (2020) Online Learning for Network Constrained Demand Response Pricing in Distribution Systems. *IEEE Transactions on Smart Grid*, **11**, 2563-2575. https://doi.org/10.1109/tsg.2019.2957705

[32] Zhao, Z., Liu, Y., Guo, L., Bai, L., Wang, Z. and Wang, C. (2023) Distribution Locational Marginal Pricing under Uncertainty Considering Coordination of Distribution and Wholesale Markets. *IEEE Transactions on Smart Grid*, **14**, 1590-1606. https://doi.org/10.1109/tsg.2022.3200704

[33] Ge, S., Li, J. and Liu, H. (2021) Peer-to-Peer Energy Trading Method for Multi-Microgrids Considering Characteristics of Smart Buildings. *Automation of Electric Power Systems*, **45**, 203-214.

[34] Yuan, G., Gao, Y. and Ye, B. (2021) Optimal Dispatching Strategy and Real-Time Pricing for Multi-Regional Integrated Energy Systems Based on Demand Response. *Renewable Energy*, **179**, 1424-1446. https://doi.org/10.1016/j.renene.2021.07.036

[35] Li, B., Shu, Q. and Liang, Y. (2019) Retrofit Planning of Urban Distribution Network for Reliable Automatic Transfer Supply. *Automation of Electric Power Systems*, **43**, 177-183.

[36] Rigo-Mariani, R. and Vai, V. (2022) An Iterative Linear DistFlow for Dynamic Optimization in Distributed Generation Planning Studies. *International Journal of Electrical Power & Energy Systems*, **138**, Article 107936. https://doi.org/10.1016/j.ijepes.2021.107936

[37] Zhang, J., Li, X., Wei, Y., Li, Z. and Lu, C. (2025) Improved Model of Limit Power Supply Capability of Flexible DC Traction Power Supply System Based on SOCP. *Proceedings of the CSEE*, **45**, 813-822.